Journal of Petroleum Science and Engineering 156 (2017) 945–957

Contents lists available at ScienceDirect

Journal of Petroleum Science and Engineering

journal homepage: www.elsevier.com/locate/petrol

# Paraffin solubility and calorimetric data calculation using Peng-Robinson EoS and modified UNIQUAC models

Vinicius M. da Silva [a], Rafael P. do Carmo [d], Felipe P. Fleming [b,c], Jean-Luc Daridon [c], Jérôme Pauly [c], F.W. Tavares [a,d,*]

[a] Escola de Química, Universidade Federal do Rio de Janeiro, Cidade Universitária, CEP: 21949-900, Rio de Janeiro, RJ, Brazil
[b] Cenpes - Centro de Pesquisas da Petrobras, Cidade Universitária, CEP: 21941-915, Rio de Janeiro, RJ, Brazil
[c] Laboratoire des Fluides Complexes et leurs Réservoirs, UPPA, France
[d] Programa de Engenharia Química/COPPE - Universidade Federal do Rio de Janeiro, Cidade Universitária, CEP: 21949-972, Rio de Janeiro, RJ, Brazil

ARTICLE INFO

*Keywords:*
Solid-liquid equilibrium
Paraffin
Differential scanning calorimetry
Peng-Robinson EoS
Solid solution model
Multisolid model

ABSTRACT

Wax deposition receives increasing attention as oil industries moves towards hostile environments. Production in deep water scenarios and even the Artic pushes the boundaries of flow assurance, especially those related to wax precipitation and deposition. Thus, modeling wax phase behavior becomes central to minimize production costs. Although different thermodynamic models are available in the literature, only the solubility curve, either entirely or only its first point, the wax appearance temperature, are used to differentiate them. It is alternatively proposed to compare these models against DSC thermograms. The results show that a liquid model based on Peng-Robinson EoS using van der Waals mixing and combining rules together with a solid model based on the modified UNIQUAC scheme can reproduce the experimental thermograms for the studied systems. As EoS's are widely used by oil companies to describe live oil fluid behavior, the proposed scheme can be readily applied to real fluids, reducing uncertainties associated to model tuning. Moreover, we show that the multiple solid solutions model, using modified UNIQUAC, presents a better description of solubility and calorimetric data when compared with the multisolid and ideal solid solution models.

## 1. Introduction

During production, petroleum is subject to different temperature and pressure conditions, which can lead to precipitation of different solids, such as hydrates, asphaltenes and waxes. Among these flow assurance issues, wax deposition gains importance as the frontier of oil exploration moves towards hostile environments, like deep water and the Artic (Huang et al., 2015). Wax deposition is hard to remediate, as it depends on mechanical removal of the deposits through pigging operations or chemical intervention like solvent soaking. As these different operations lead to production loss, the most cost effective strategy to deal with wax deposition is to avoid it during the design of production installations (Azevedo and Teixeira, 2003). Therefore, one is obliged to use wax deposition models, which depend either on the amount of wax precipitated or on its derivative with respect to temperature. Both can be calculated through thermodynamic models of solid-liquid equilibria (SLE) of waxes and oil (Azevedo and Teixeira, 2003).

Modeling wax behavior in solid phase has been the aim of study of several works in the literature (Banki et al., 2008; Ji et al., 2004). A variety of solid paraffins models have been developed, e.g., the multisolid model, which describes solid paraffins as being multiple pure solid phases, the ideal solid solution model, which describes paraffinic solid phase as being an ideal solution, and other models that describe solid paraffins as one or more non-ideal solid phase solutions, the solid solution models (Lira-Galeana et al., 1996; Won, 1986; Hansen et al., 1988; Coutinho et al., 2006).

Such as solid phases, liquid phases may also be modelled in different ways. Excess Gibbs energy (EGE) models, also called activity coefficient models, as well as cubic equations of state (EoS), are commonly used to describe liquid phases. Activity coefficient approaches are known for their good agreement to liquid behavior. On the other hand, there is no substantial information about the use of EoS with van der Waals mixing rule along with EGE models for solids. However, since this last liquid model presents many advantages when compared to activity coefficient models, e.g., possibility of tuning the thermodynamic model from PVT data and taking into account pressure effect, making the model

* Corresponding author. Escola de Química, Universidade Federal do Rio de Janeiro, Cidade Universitária, CEP: 21949-900, Rio de Janeiro, RJ, Brazil.
*E-mail address:* tavares@eq.ufrj.br (F.W. Tavares).

http://dx.doi.org/10.1016/j.petrol.2017.06.064
Received 5 December 2016; Received in revised form 6 June 2017; Accepted 28 June 2017
Available online 1 July 2017

applicable to live oils, determining EoS efficiency in modelling liquids is of great interest.

Usually, validation of SLE modelling is carried out by comparing calculated results with wax appearance temperature (WAT) experimental data, and thermodynamic models available in the literature are tuned using this approach. Nevertheless, the WAT cannot be considered a true equilibrium point, since its value has a strong dependency on the experimental procedure used (Ji et al., 2004; Coutinho and Daridon, 2005). The true equilibrium point is, actually, the wax disappearance temperature (WDT), which is the variable calculated from the thermodynamic models. Hence, tuning thermodynamic models based on the WAT turn up to be a questionable strategy (Fleming et al., 2017).

An alternative approach consists in tuning the thermodynamic model directly to DSC (Differential Scanning Calorimetry) thermograms, as proposed by Fleming et al. (2017). In this strategy, instead of fitting the model parameters to solubility or WAT data, they are fitted to DSC curves. For this purpose, Fleming et al. (2017) have investigated the use of a simplified method for the simulation of DSC thermograms, which only takes into consideration the independent transition enthalpies of the different components, neglecting excess enthalpy contributions, and uses an incompressible model for the liquid phase. Aiming at a more accurate and widely applicable approach, non-idealities should also be contemplated in heat calculations used to build up simulated DSC thermograms, as well as a different liquid model.

To assure a rigorous and widely applicable calculation scheme for the DSC thermograms, a complete energy balance of the system, taking into consideration solid and liquid phases, is performed. It is set as reference for all components in all phases the ideal gas state, which makes the energy balance suitable for multiphase systems. For the liquid phase, Peng-Robinson EoS has been used (Peng and Robinson, 1976). It was compared to the Flory free-volume combined with modified UNIFAC model used by Fleming et al. (2017). Three different solid models, the multisolid, ideal solid solution and solid solution, were also compared. To validate the proposed approach, the results were compared to experimental data of five synthetic mixtures at atmospheric pressure (Fleming et al., 2017; Dauphin et al., 1999).

## 2. Methodology

### 2.1. DSC simulation

Differential Scanning Calorimetry (DSC) is an experimental method that measures the heat flow related with transitions in materials as a function of time (Chiavaro, 2015). When carried out at a constant temperature rate, one can easily convert the results from a time dependence to a temperature dependence basis.

For simulation purposes, the heat flux measured in the DSC can be calculated taking into consideration that at a constant pressure the heat exchanged is equal to the product between the system molar enthalpy variation, $\overline{H}$, and the total number of moles of the sample, *Nmol*, as in

$$\frac{\delta Q}{\delta t} = \frac{\partial \overline{H}}{\partial t} Nmol. \tag{1}$$

The molar enthalpy derivative with time is related to its derivative with temperature through

$$\frac{\partial \overline{H}}{\partial t} = \frac{\partial \overline{H}}{\partial T}\frac{\partial T}{\partial t}. \tag{2}$$

To reduce the transient effects in the DSC experiment, a small value of the temperature rate, $\frac{\partial T}{\partial t}$, should be adopted (Fleming et al., 2017; Hansen et al., 1991). A rate of 0.2 °C/min was used by Fleming et al. (2017) for all the DSC experiments studied in this work. Therefore, for DSC simulation, it is just necessary the evaluation of the molar enthalpy derivative with the temperature, $\frac{\partial \overline{H}}{\partial T}$. This derivative has been calculated numerically as follows:

$$\frac{\partial \overline{H}}{\partial T} = \frac{\overline{H}(T+\Delta T) - \overline{H}(T-\Delta T)}{2\Delta T}. \tag{3}$$

The total molar enthalpy, $\overline{H}$, is obtained from the molar enthalpy of each phase present in the mixture:

$$\overline{H} = \sum_{j=1}^{Np} \beta^n \overline{H}^n, \tag{4}$$

where *Np*, $\beta^n$ and $\overline{H}^n$ are the number of phases, the phase fraction and the molar enthalpy of phase *n*, respectively.

A complete thermodynamic path has been proposed in order to calculate the molar enthalpy of each pure component *i* in each phase in the mixture, which can then be combined to give the molar enthalpy of the different phases. The path starts at the ideal gas reference state at $T_0 = 298$ K and $P_0 = 1$ atm, and ends at solid state at the system's temperature, *T*, and pressure, *P*, as shown in Fig. 1. As a wide range of n-alkanes present solid-solid transitions before melting (Ji et al., 2004; Coutinho et al., 1995, 2006), it is also encompassed by the proposed path.

In Fig. 1, $T^f$, $P^f$, $T^{tr}$ and $P^{tr}$ are the melting temperature, melting pressure, temperature of crystalline transition and pressure of crystalline transition of pure paraffins, respectively. The different numbers in Fig. 1 indicate the molar enthalpy of component *i* in the different states connected in the proposed path. Eqs. (5)–(14) give the molar enthalpy variation that connects the different states, respectively, and are represented as $\overline{H}^1_{i,pure} - \overline{H}^0_{i,pure}$, $\overline{H}^2_{i,pure} - \overline{H}^1_{i,pure}$ and so on.

$$\overline{H}^1_{i,pure} - \overline{H}^0_{i,pure} = \int_{T_0}^{T} Cp^{ig}_{i,pure} dT \tag{5}$$

$$\overline{H}^2_{i,pure} - \overline{H}^1_{i,pure} = \int_{P_0}^{P} \left[ \overline{V}^{ig}_{i,pure} - T\left(\frac{\partial \overline{V}^{ig}_{i,pure}}{\partial T}\right)_P \right] dP = 0 \tag{6}$$

$$\overline{H}^3_{i,pure} - \overline{H}^2_{i,pure} = \overline{H}^L_{i,pure}(T,P) - \overline{H}^{ig}_{i,pure}(T,P) = \overline{H}^R_{i,pure}(T,P) \tag{7}$$

$$\overline{H}^4_{i,pure} - \overline{H}^3_{i,pure} = \int_{P}^{P^f} \left[ \overline{V}^L_{i,pure} - T^f_i \left(\frac{\partial \overline{V}^L_{i,pure}}{\partial T}\right)_P \right] dP \tag{8}$$

$$\overline{H}^5_{i,pure} - \overline{H}^4_{i,pure} = \int_{T}^{T^f_i} Cp^L_{i,pure} dT \tag{9}$$

$$\overline{H}^6_{i,pure} - \overline{H}^5_{i,pure} = -\Delta \overline{H}^f_{i,pure} \tag{10}$$

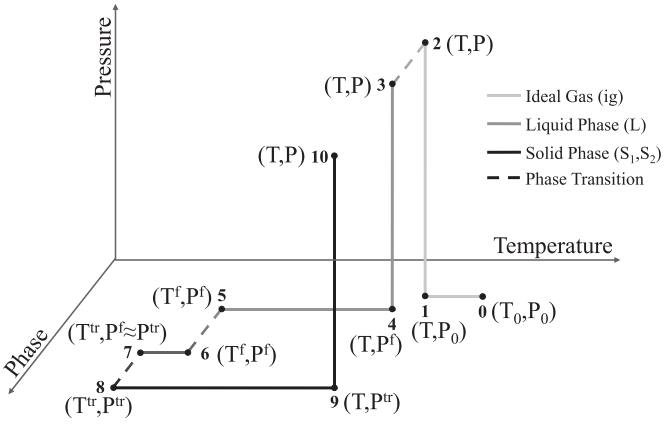


**Fig. 1.** Thermodynamic path used to obtain the molar enthalpy of pure paraffins.

$$\overline{H}^{7}_{i,pure} - \overline{H}^{6}_{i,pure} = \int_{T_i^f}^{T_i^{tr}} Cp^{S_1}_{i,pure} dT \tag{11}$$

$$\overline{H}^{8}_{i,pure} - \overline{H}^{7}_{i,pure} = -\Delta\overline{H}^{tr}_{i,pure} \tag{12}$$

$$\overline{H}^{9}_{i,pure} - \overline{H}^{8}_{i,pure} = \int_{T_i^{tr}}^{T} Cp^{S_2}_{i,pure} dT \tag{13}$$

$$\overline{H}^{10}_{i,pure} - \overline{H}^{9}_{i,pure} = \int_{P_i^{tr}}^{P} \left[ \overline{V}^{S_2}_{i,pure} - T_i^f \left( \frac{\partial \overline{V}^{S_2}_{i,pure}}{\partial T} \right)_P \right] dP \tag{14}$$

In Eqs. (5)–(14), $Cp^{ig}_{i,pure}$ and $\overline{V}^{ig}_{i,pure}$ are the heat capacity and the molar volume of pure component $i$ as an ideal gas, respectively. $Cp^{L}_{i,pure}$ is the heat capacity of pure component $i$ in the liquid phase. $\overline{H}^{R}_{i,pure}$ is the molar residual enthalpy of pure component $i$, which is calculated from an EoS. $\overline{V}^{L}_{i,pure}$ is the molar volume of pure component $i$ in the liquid phase. $\Delta\overline{H}^{f}_{i,pure}$ and $\Delta\overline{H}^{tr}_{i,pure}$ are the molar melting enthalpy of pure component $i$ and the molar transition enthalpy between the solid states $S_1$ and $S_2$, respectively. $\overline{V}^{S_1}_{i,pure}$ and $\overline{V}^{S_2}_{i,pure}$ are the molar volumes of pure component $i$ in the solid states $S_1$ and $S_2$, respectively. $Cp^{S_1}_{i,pure}$ and $Cp^{S_2}_{i,pure}$ are the heat capacities of pure component $i$ in the solid states $S_1$ and $S_2$, respectively.

Considering $Cp^{S_1}_{i,pure}$ and $Cp^{S_2}_{i,pure}$ similar (Ji et al., 2004; Coutinho et al., 1995), one gets:

$$Cp^{S_1}_{i,pure} = Cp^{S_2}_{i,pure} = Cp^{S}_{i,pure}. \tag{15}$$

Then, the terms $\int_{T_i^f}^{T_i^{tr}} Cp^{S_1}_{i,pure} dT$ and $\int_{T_i^{tr}}^{T} Cp^{S_2}_{i,pure} dT$ are grouped and added to Eqs. (9), (10) and (12), resulting in

$$\overline{H}^{9}_{i,pure} - \overline{H}^{4}_{i,pure} = \int_{T_i^f}^{T} \left( Cp^{S}_{i,pure} - Cp^{L}_{i,pure} \right) dT - \Delta\overline{H}^{f}_{i,pure} - \Delta\overline{H}^{tr}_{i,pure}. \tag{16}$$

Since enthalpies of phase transition are many orders of magnitude greater than the integrals of heat capacities difference for the temperatures of interest in petroleum production, the integral in Eq. (16) has been neglected. Thus, for a pure component $i$, the molar enthalpy in the solid phase is

$$\begin{aligned} \overline{H}^{S}_{i,pure}(T,P) = {} & \overline{H}^{ig}_{i,pure}(T_0,P_0) + \int_{T_0}^{T} Cp^{ig}_{i,pure} dT + \overline{H}^{R}_{i,pure}(T,P) - \Delta\overline{H}^{f}_{i,pure} \\ & - \Delta\overline{H}^{tr}_{i,pure} + \int_{P}^{P_i^f} \left[ \left( \overline{V}^{S}_{i,pure} - \overline{V}^{L}_{i,pure} \right) \right. \\ & \left. - T_i^f \left( \frac{\partial \left( \overline{V}^{S}_{i,pure} - \overline{V}^{L}_{i,pure} \right)}{\partial T} \right)_P \right] dP \end{aligned} \tag{17}$$

Moreover, the term related to pressure variation of condensed phase is very small once $\overline{V}^{L}_{i} \approx \overline{V}^{S}_{i}$ and then have also been neglected. Therefore, the molar enthalpy of an ideal solid phase with composition $\underline{x}^S$ is

$$\begin{aligned} \overline{H}^{S,ideal}(T,P,\underline{x}^S) = {} & \sum_{i=1}^{Nc} x_i^S \overline{H}^{ig}_{i,pure}(T_0,P_0) + \sum_{i=1}^{Nc} x_i^S \int_{T_0}^{T} Cp^{ig}_{i,pure} dT \\ & + \overline{H}^{R}(T,P,\underline{x}^S) - \sum_{i=1}^{Nc} x_i^S \Delta\overline{H}^{f}_{i,pure} - \sum_{i=1}^{Nc} x_i^S \Delta\overline{H}^{tr}_{i,pure} \end{aligned} \tag{18}$$

The molar enthalpy of the liquid phase is:

$$\begin{aligned} \overline{H}^{L}(T,P,\underline{x}^L) = {} & \sum_{i=1}^{Nc} x_i^L \overline{H}^{ig}_{i,pure}(T_0,P_0) + \sum_{i=1}^{Nc} x_i^L \int_{T_0}^{T} Cp^{ig}_{i,pure} dT \\ & + \overline{H}^{R}(T,P,\underline{x}^L), \end{aligned} \tag{19}$$

where $\overline{H}^{R}$ is obtained from the Peng-Robinson EoS. For the ideal gas heat capacities calculation, $Cp^{ig}_{i,pure}$, the parameters of the correlation presented by Passut and Danner (1972), originally developed using data from $CH_4$ to $C_{20}H_{44}$, have been correlated and extrapolated for n-alkanes with longer chains. Here, the ideal gas molar enthalpy at the reference state for each pure component $i$, $\overline{H}^{ig}_{i,pure}(T_0, P_0)$, is set to zero.

Solid phase non-idealities are taken into account through the incorporation of the excess molar enthalpy, $\overline{H}^{E}$:

$$\overline{H}^{S}(T,P,\underline{x}^S) = \overline{H}^{S,ideal}(T,P,\underline{x}^S) + \overline{H}^{E}(T,\underline{x}^S), \tag{20}$$

where

$$\overline{H}^{E}(T,\underline{x}^S) = -RT^2 \sum_{i=1}^{Nc} x_i^S \left( \frac{\partial \ln \gamma_i^S}{\partial T} \right)_{P,x}. \tag{21}$$

In Eq. (21), the activity coefficient derivative of component $i$ in the solid phase is obtained analytically from the modified UNIQUAC model (Coutinho et al., 2006).

### 2.2. Thermodynamic model

The thermodynamic model used to determinate the amount of paraffins precipitated and the compositions of the phases in the mixture is based on the multiple solid solutions model proposed by Coutinho et al. (2006).

Coutinho's model (Coutinho et al., 2006) employs a combination of modified UNIFAC (Larsen et al., 1987) and Flory free-volume (Coutinho et al., 1995) models to describe the liquid phase non-idealities, and the modified UNIQUAC model to describe the solid phase non-idealities.

The usage of Peng-Robinson EoS to describe liquid phase non-idealities arises as an alternative proposed in this paper. In comparison to an activity coefficient model, the Peng-Robinson EoS has the advantage of being already widely used by oil industry, as it can be tuned from PVT data and takes into account pressure effect, making it easier to model live oils. In this work, Peng-Robinson EoS was used together with the classical van der Waals mixing and combining rules, in which the binary interaction coefficient, $k_{ij}$, is calculated using the correlation proposed by Pan et al. (1997) and $l_{ij} = 0$. The critical properties and acentric factors of all components used in this work are estimated using the correlations suggested by Marano and Holder (1997).

For the solid solution model, if the phases are in equilibrium, the condition of equal fugacities must be satisfied for each component $i$:

$$\widehat{f}_i^{L}(T,P,\underline{x}^L) = \widehat{f}_i^{S}(T,P,\underline{x}^S). \tag{22}$$

In the model of Coutinho (Coutinho et al., 2006), the liquid and solid fugacities $\widehat{f}_i^{L}$ and $\widehat{f}_i^{S}$ are:

$$\widehat{f}_i^{L}(T,P,\underline{x}^L) = x_i^L \gamma_i^L f_i^L \tag{23}$$

and

$$\widehat{f}_i^{S}(T,P,\underline{x}^S) = x_i^S \gamma_i^S f_i^S, \tag{24}$$

in which pure solid fugacity, $f_i^S$, is calculated from the pure liquid fugacity, $f_i^L$:

$$\ln\left(\frac{f_i^L}{f_i^S}\right) = \frac{\Delta\overline{H}^{f}_{i,pure}}{RT_i^f}\left(\frac{T_i^f}{T} - 1\right) + \frac{\Delta\overline{H}^{tr}_{i,pure}}{RT_i^{tr}}\left(\frac{T_i^{tr}}{T} - 1\right). \tag{25}$$

The SLE ratio, $K_i^{SL}$, is obtained by:

$$K_i^{SL} = \frac{x_i^S}{x_i^L} = \frac{\gamma_i^L}{\gamma_i^S} \exp\left[\frac{\Delta\overline{H}_{i,pure}^{f}}{RT_i^f}\left(\frac{T_i^f}{T} - 1\right) + \frac{\Delta\overline{H}_{i,pure}^{tr}}{RT_i^{tr}}\left(\frac{T_i^{tr}}{T} - 1\right)\right]. \quad (26)$$

The same correlations used by Coutinho et al. (2006) are employed to calculate the transition and fusion properties.

As aforementioned, Coutinho et al. (2006) calculated the liquid activity coefficient, $\gamma_i^L$, combining the modified UNIFAC model, $\gamma_i^{res}$, with the Flory free-volume model, $\gamma_i^{comb-fv}$:

$$\ln \gamma_i^L = \ln \gamma_i^{res} + \ln \gamma_i^{comb-fv}. \quad (27)$$

The activity coefficient of the solid phase, $\gamma_i^S$, is calculated using the modified UNIQUAC model,

$$\frac{\overline{G}^E}{RT} = \sum_{i=1}^{Nc} x_i^s \ln\left(\frac{\Phi_i}{x_i^s}\right) + \frac{Z}{2}\sum_{i=1}^{Nc} q_i x_i^s \ln\left(\frac{\theta_i}{\Phi_i}\right) - \sum_{i=1}^{Nc} q_i x_i^s \ln\left[\sum_{j=1}^{Nc} \theta_j \tau_{ji}\right], \quad (28)$$

in which $\overline{G}^E$ is the EGE per mole of mixture and $Nc$ is the number of components in the mixture.

The parameters $\tau_{ji}$, $\theta_i$ and $\Phi_i$ are calculated as follow:

$$\tau_{ji} = \exp\left(-\frac{\lambda_{ji} - \lambda_{ii}}{q_i RT}\right), \quad (29)$$

$$\theta_i = \frac{x_i^S q_i}{\sum_{j=1}^{Nc} x_j^S q_j} \quad (30)$$

and

$$\Phi_i = \frac{x_i^S r_i}{\sum_{j=1}^{Nc} x_j^S r_j}. \quad (31)$$

The structural parameters of pure components, $r_i$ and $q_i$, are obtained from the parameter table of the original UNIFAC model (Abrams and Prausnitz, 1975):

$$r_i = 0.6744 CN_i + 0.4534 \quad (32)$$

and

$$q_i = 0.540 CN_i + 0.616, \quad (33)$$

where $CN_i$ is the number of carbon atoms of component $i$.

The activity coefficient is defined as

$$RT \ln \gamma_i = \left(\frac{\partial\left(n_T \overline{G}^E\right)}{\partial n_i}\right)_{T,P,n_j(j\neq i)}, \quad (34)$$

then the expression derived for $\gamma_i^S$ is

$$\ln \gamma_i^S = \ln\left(\frac{\Phi_i}{x_i^S}\right) + 1 - \frac{\Phi_i}{x_i^S} - \frac{Z}{2} q_i \left(\ln\left(\frac{\Phi_i}{\theta_i}\right) + 1 - \frac{\Phi_i}{\theta_i}\right) + q_i - q_i \ln\left(\sum_{j=1}^{Nc} \theta_j \tau_{ij}\right) - q_i \sum_{j=1}^{Nc} \frac{\theta_j \tau_{ij}}{\sum_{w=1}^{Nc} \theta_w \tau_{wj}}. \quad (35)$$

For two identical paraffins, the pair interaction energies, $\lambda_{ii}$, are (Coutinho et al., 2006):

$$\lambda_{ii} = -\frac{2}{Z}\left(\Delta\overline{H}_{i,pure}^{sub} - RT\right), \quad (36)$$

where the coordination number, $Z$, is set to 10. The heat of sublimation, $\Delta\overline{H}_{i,pure}^{sub}$, for each pure component $i$ is calculated as (Coutinho et al., 2006)

$$\Delta\overline{H}_{i,pure}^{sub} = \Delta\overline{H}_{i,pure}^{vap} + \Delta\overline{H}_{i,pure}^{f} + \Delta\overline{H}_{i,pure}^{tr}, \quad (37)$$

in which the heat of vaporization, $\Delta\overline{H}_{i,pure}^{vap}$, is calculated using the correlation proposed by Morgan and Kobayashi (1994).

For two different paraffins, the interaction energy, $\lambda_{ij}$, is defined by Eq. (38), where the component $j$ is the n-alkane with the shorter chain of the pair $ij$ (Coutinho et al., 1996).

$$\lambda_{ij} = \lambda_{ji} = \lambda_{jj} \quad (38)$$

According to the methodology developed by Fleming et al. (2017), the value of $\lambda_{ij}$ is used to tune the thermodynamic model in order to make the DSC simulation match the experimental data, as showed in Eq. (39). The parameter used to tune the thermodynamic model is represented by $\Delta\lambda$ and the method of Hooke and Jeeves (1961) is employed for the parameter estimation. This parameter will directly affect phase equilibrium by means of the solid activity coefficient, altering equilibrium compositions, phase fractions and, consequently, the system's enthalpy. If $\Delta\lambda = 0$, the model returns the original result and the calculation is completely predictive.

$$\lambda_{ij}^{adjust} = \lambda_{ij}(1 + \Delta\lambda) \quad (39)$$

The ideal solid solution method imposes that $\gamma_i^S$ in Eq. (24) is unitary, predicting the formation of only one solid phase. Hence, the excess enthalpy is neglected in the solid enthalpy calculation, Eq. (20), although the effect of the presence of different paraffins in the same phase is accounted by the enthalpy of ideal phase term.

For the multisolid model, each paraffin precipitates in a pure phase. This way, the solid composition will always be unitary and Eq. (24) will reduce to the pure solid fugacity, being calculated based on the fugacity of pure liquid, Eq. (25). This model also does not take into consideration the excess enthalpy influence in Eq. (20). Furthermore, the enthalpy of ideal phase term is calculated by summing the enthalpy of each pure solid phase.

Adopting the Peng-Robinson EoS for liquid phase description, the liquid fugacity is:

$$\widehat{f}_i^L(T, P, \underline{x}^L) = x_i^L \widehat{\varphi}_i^L P, \quad (40)$$

where $\widehat{\varphi}_i^L$ is the fugacity coefficient of component $i$. The SLE ratio then becomes:

$$K_i^{SL} = \frac{x_i^S}{x_i^L} = \frac{\widehat{\varphi}_i^L}{\varphi_i^L \gamma_i^S} \exp\left[\frac{\Delta\overline{H}_{i,pure}^{f}}{RT_i^f}\left(\frac{T_i^f}{T} - 1\right) + \frac{\Delta\overline{H}_{i,pure}^{tr}}{RT_i^{tr}}\left(\frac{T_i^{tr}}{T} - 1\right)\right], \quad (41)$$

where $\varphi_i^L$ is the fugacity coefficient of component $i$ as a pure liquid calculated from the Peng-Robinson EoS.

### 2.3. Phase equilibrium algorithm

To calculate DSC and solubility curves, it is first necessary to determine the existing phases in the system and to converge the compositions and fractions of each phase at the given temperature and pressure. Thus, to accomplish this task, it was developed a calculation structure, presented in Fig. 2.

Taking the liquid as the reference phase, the algorithm searches for a solid phase by carrying out a stability analysis. If the test points out that there is a new stable solid phase, then a flash calculation is performed to converge the system. These coupled actions are repeated until the stability analysis does not find a new stable solid phase. When it happens, the weight fraction of solid is calculated using

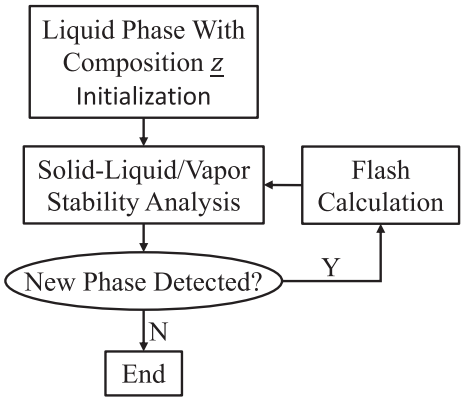


**Fig. 2.** Phase equilibrium strategy scheme.

$$wt(\%) = \frac{\sum_{i=1}^{Nc}\sum_{j=1}^{Nps} x_i^j \beta^j MW_i}{\sum_{i=1}^{Nc}\sum_{j=1}^{Np} x_i^j \beta^j MW_i}, \tag{42}$$

where $MW_i$ and $Nps$ are, respectively, the molecular weight of component $i$ and the number of solid phases, and the simulation is concluded.

### 2.3.1. Flash calculation

To calculate the phase equilibrium with fixed temperature and pressure, the $Np-1$ phase fractions and all compositions were calculated using, respectively, Newton's and successive substitution methods.

As shown in Fig. 3, first the K-factors are obtained by

$$K_i^n = \frac{\widehat{\varphi}_i^L}{\varphi_i^L \gamma_i^{S_n}} exp\left[\frac{\Delta\overline{H}_{i,pure}^f}{RT_i^f}\left(\frac{T_i^f}{T}-1\right) + \frac{\Delta\overline{H}_{i,pure}^{tr}}{RT_i^{tr}}\left(\frac{T_i^{tr}}{T}-1\right)\right] \tag{43}$$

for solid phases. The superscript $S_n$ represents the $n^{\text{th}}$ solid phase. As we considered that the solvent does not precipitate, its K-factor for solid phases is automatically set to zero.

The $Np-1$ residuals of the Newton method, $\underline{F}$, were calculated by the expression (Ziervogel and Poling, 1983)

$$F^n = \sum_{i=1}^{Nc} x_i^L K_i^n - 1 \tag{44}$$

and their derivatives with respect to the $m^{\text{th}}$ phase fraction by

$$\frac{\partial F^n}{\partial \beta^m} = \sum_{i=1}^{Nc} \frac{x_i^n\left(x_i^L - x_i^m\right)}{z_i}. \tag{45}$$

The system of equations

$$\frac{\partial \underline{F}}{\partial \underline{\beta}} \cdot \Delta\underline{\beta} = \underline{F} \tag{46}$$

is then solved, where $\Delta\underline{\beta}$ is the difference between phase fractions in the current iteration and in the next one. Thus, $\underline{\beta}$ is updated subtracting it by the step, $\Delta\underline{\beta}$, just calculated and, after this, the compositions, $\underline{x}$, are updated according to the mass balance:

$$x_i^L = \frac{z_i}{1 + \sum_{n=1}^{Np}\beta^n\left(K_i^n - 1\right)} \tag{47}$$

and

$$x_i^n = \frac{z_i K_i^n}{1 + \sum_{n=1}^{Np}\beta^n\left(K_i^n - 1\right)} \tag{48}$$

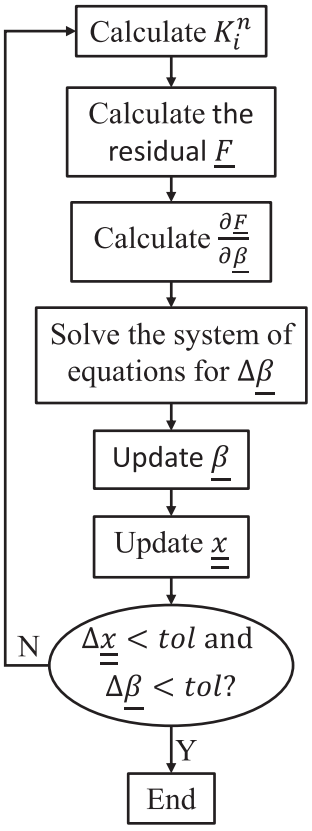


**Fig. 3.** Box diagram of the Flash calculation algorithm.

The convergence criteria is based on the maximum step applied to $\underline{\beta}$ and $\underline{x}$. Unless it's lower than a specified tolerance, the routine is executed again.

### 2.3.2. Stability analysis

The tangent plane distance to the Gibbs energy surface criterion (TPD) (Michelsen, 1982) was used to search for solid phases. It was carried out by minimizing the following equation:

$$tm = 1 + \sum_{i=1}^{Nc} W_i\left[ln(W_i) + ln\left(\gamma_i^S(T,\underline{W})\right) + ln\left(\varphi_i^L(T,P)\right) - d_i - 1\right], \tag{49}$$

where

$$d_i = ln\left(x_i^L\right) + ln\left(\widehat{\varphi}_i^L(T,P,\underline{x}^L)\right), \tag{50}$$

$\underline{W}$ is a stability variable that simulates the phase composition and $tm$ is the modified tangent plane distance, which is an alternative way of expressing the TPD.

The stability analysis begins with the initialization of $Nc$ trials phases, each one rich in one compound. If it is known that some component certainly will not precipitate, the number of trial phases may be reduced.

Next, the successive substitution method is applied to solve the system of equations (Michelsen, 1982) constituted by the gradient of Eq. (49), also written as

$$W_i = exp\left(d_i - ln\left(\gamma_i^S(T,\underline{W})\right) - ln\left(\varphi_i^L(T,P)\right)\right). \tag{51}$$

In the end of the method, it should be tested if the trial phases are converging to already existing solid phases, what can be accomplished by testing if

$$\sum_{i=1}^{Nc}\left|W_i - x_i^L\right| < tol. \tag{52}$$

The phases seeming to converge to already existing solid phases are excluded from the search. Whenever the remaining solid trial phases are not converged after the successive substitution method, Newton's method should be utilized (Michelsen, 1982).

The gradient and the Hessian are calculated as follows:

$$\frac{\partial tm}{\partial \varepsilon_i} = \sqrt{W_i}\left[ln(W_i) + ln\left(\gamma_i^S(T,\underline{W})\right) + ln\left(\varphi_i^L(T,P)\right) - d_i\right] \tag{53}$$

and

$$\frac{\partial^2 tm}{\partial \varepsilon_i \partial \varepsilon_j} = \sqrt{W_i W_j}\,\frac{\partial ln\left(\gamma_i^S(T,\underline{W})\right)}{\partial W_j} + \delta_{ij}\left[1 + \frac{1}{2\varepsilon_i}\frac{\partial tm}{\partial \varepsilon_i}\right], \tag{54}$$

where $\delta_{ij}$ is the kronecker delta and $\varepsilon_i$ is $2\sqrt{W_i}$. After Newton's method, the solid trial phases must be once more compared to the already existing solid phases as it was done after the successive substitution method.

Once the trial phases have converged, the stability variable, $W_{Total}$, which is directly connected to the *tm*, must be calculated:

$$W_{Total} = \sum_{i=1}^{Nc} W_i. \tag{55}$$

In case $W_{Total}$ value is greater than unity, the system is considered unstable, hence the corresponding trial phase must be included in it. Otherwise, the system remains unaltered.

## 3. Data

Experimental composition and DSC thermograms for five synthetic mixtures presented by Fleming et al. (2017) were used to simulate the DSC and solubility curves. These mixtures are composed of one continuous series ranging from $C_{18}$ to $C_{36}$, and four bimodal distributions obtained by removing a defined number of intermediate paraffins. The WDT and the solubility data of these synthetic mixtures were measured by Dauphin et al. (1999) and are also used. Table 1 shows the composition data of the studied mixtures. The name of each mixture is the same given by Dauphin et al. (1999).

**Table 1**
Compositions for the synthetic mixtures studied (% mass) (Fleming et al., 2017).

| Component | *Bim 0* | *Bim 3* | *Bim 5* | *Bim 9* | *Bim 13* |
|---|---|---|---|---|---|
| *n*-$C_{10}$ | 63.90 | 64.25 | 64.65 | 65.63 | 66.4 |
| *n*-$C_{18}$ | 4.285 | 4.922 | 5.362 | 6.967 | 10.6 |
| *n*-$C_{19}$ | 3.844 | 4.419 | 4.874 | 6.289 | 9.65 |
| *n*-$C_{20}$ | 3.473 | 3.944 | 4.388 | 5.684 | 8.71 |
| *n*-$C_{21}$ | 3.116 | 3.550 | 4.072 | 5.103 | – |
| *n*-$C_{22}$ | 2.789 | 3.213 | 3.541 | 4.601 | – |
| *n*-$C_{23}$ | 2.507 | 2.883 | 3.172 | – | – |
| *n*-$C_{24}$ | 2.254 | 2.656 | 2.824 | – | – |
| *n*-$C_{25}$ | 2.001 | 2.337 | – | – | – |
| *n*-$C_{26}$ | 2.006 | – | – | – | – |
| *n*-$C_{27}$ | 1.595 | – | – | – | – |
| *n*-$C_{28}$ | 1.442 | – | – | – | – |
| *n*-$C_{29}$ | 1.263 | 1.436 | – | – | – |
| *n*-$C_{30}$ | 1.120 | 1.277 | 1.442 | – | – |
| *n*-$C_{31}$ | 0.991 | 1.145 | 1.248 | – | – |
| *n*-$C_{32}$ | 0.877 | 1.000 | 1.115 | 1.444 | – |
| *n*-$C_{33}$ | 0.802 | 0.887 | 1.002 | 1.279 | – |
| *n*-$C_{34}$ | 0.694 | 0.787 | 0.865 | 1.128 | 1.723 |
| *n*-$C_{35}$ | 0.515 | 0.681 | 0.760 | 0.997 | 1.521 |
| *n*-$C_{36}$ | 0.530 | 0.617 | 0.682 | 0.880 | 1.377 |

## 4. Results and discussion

### 4.1. DSC simulation, Peng-Robinson EoS evaluation and parameter estimation

All the experimental DSC thermograms showed in this paper have been measured under cooling regime (Fleming et al., 2017). The first peak presented in all five thermograms is called supersaturation peak, which occur due to kinetic effects (Fleming et al., 2017). Once the focus is only the thermodynamics available in these DSC thermograms, these peaks will not be taken into consideration. As the experiments have been carried out under cooling regime, the temperature in which the supersaturation peak appears is the measured WAT. The second peak observed in the mixtures *Bim 3*, *Bim* 5, *Bim* 9 and *Bim* 13 corresponds to the precipitation of a phase rich in the second group of paraffins in the bimodal

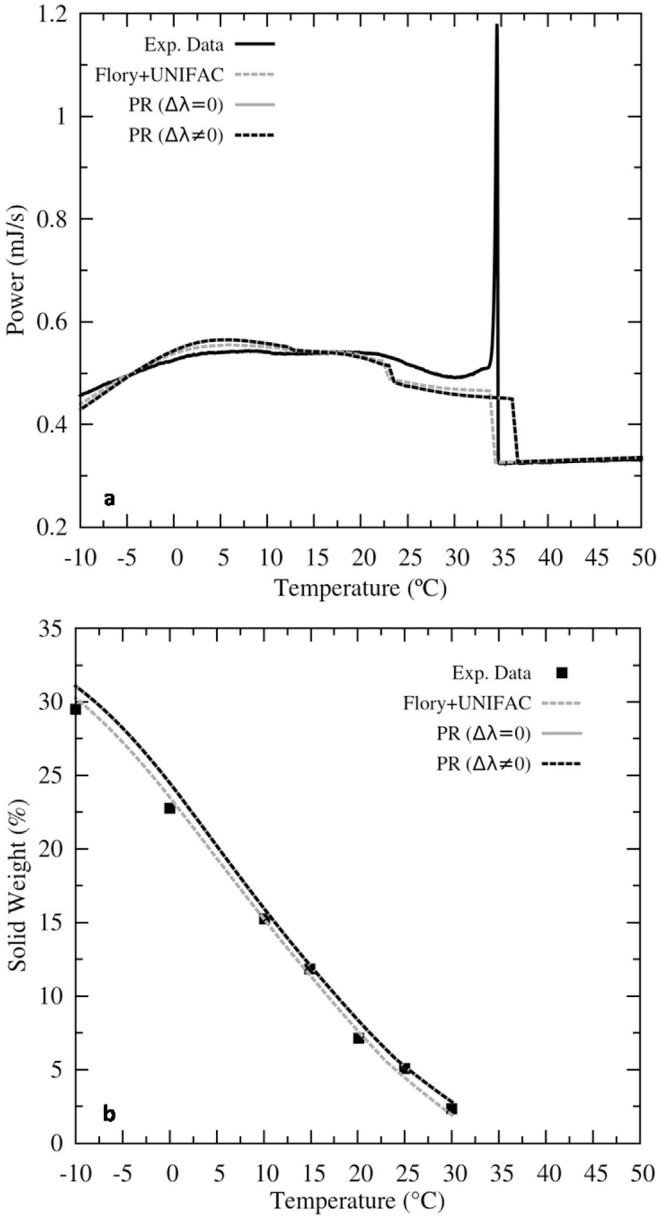


**Fig. 4.** Bim 0 **(a)** DSC and **(b)** Solubility data description using three different approaches: modified UNIQUAC for solid phases and Peng-Robinson EoS for the liquid phase; modified UNIQUAC for solid phases and Flory + UNIFAC for the liquid phase; modified UNIQUAC with estimated $\Delta\lambda$ for solid phases and Peng-Robinson EoS for the liquid phase.

distributions.

Experimental and calculated DSC thermograms and solubility curves for the five mixtures studied are displayed in Figs. 4–8. The results were named Flory + UNIFAC, as studied by Coutinho et al. (2006), which means that the models of Flory free-volume combined with modified UNIFAC are used for the liquid phase, and PR, for the proposed Peng-Robinson EoS for the liquid phase. For the PR results, the curves obtained with the parameter $\Delta\lambda = 0$ and $\Delta\lambda$ estimated ($\Delta\lambda \neq 0$) are presented. For all cases, the UNIQUAC model has been used for the solid phase.

Parameter $\Delta\lambda$ was estimated by minimizing the squared error between the experimental and the calculated DSC signals. The results showed that selecting points at indiscriminately lower temperatures than the WAT would most of the times lead to a local minimum, where perfect fit of the thermograms' second peak is achieved. This happens because, since the slope of the curve in this region is greater than in most of the thermogram, a small deviation of a point near there would cause the objective function to sorely increase, while away from there errors would be underrated. To avoid this behavior, only points at least 2.5 °C distant from the peaks were used. Parameter estimation was carried out using about forty points, parameter step set to $10^{-5}$ and the search range fixed between −0.1 and 0.1. Table 2 shows the parameter estimation results using the PR EoS for the liquid phase.

The calculated and experimental values of WDT for the thermodynamic models studied and the deviations between these values are shown in Tables 3 and 4, respectively.

The results for *Bim* 0 displayed in Fig. 4 show that the models Flory + UNIFAC and PR do not differ considerably, and are in good agreement with the experimental DSC data. Since the estimated parameter $\Delta\lambda$ for this mixture was very small, both results for PR model were the same. The Flory + UNIFAC model predicted exactly the value of WAT measured from DSC, whereas the PR model predicted a little higher value. The WAT

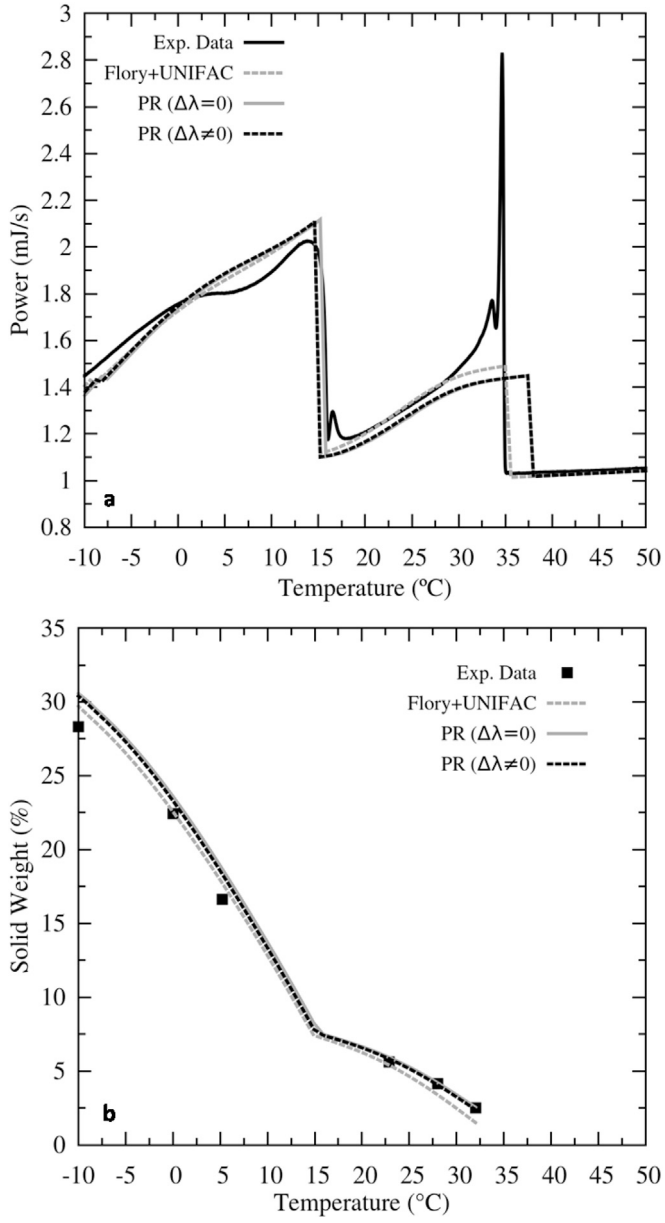


**Fig. 5.** Bim 3 **(a)** DSC and **(b)** Solubility data description using three different approaches: modified UNIQUAC for solid phases and Peng-Robinson EoS for the liquid phase; modified UNIQUAC for solid phases and Flory + UNIFAC for the liquid phase; modified UNIQUAC with estimated $\Delta\lambda$ for solid phases and Peng-Robinson EoS for the liquid phase.

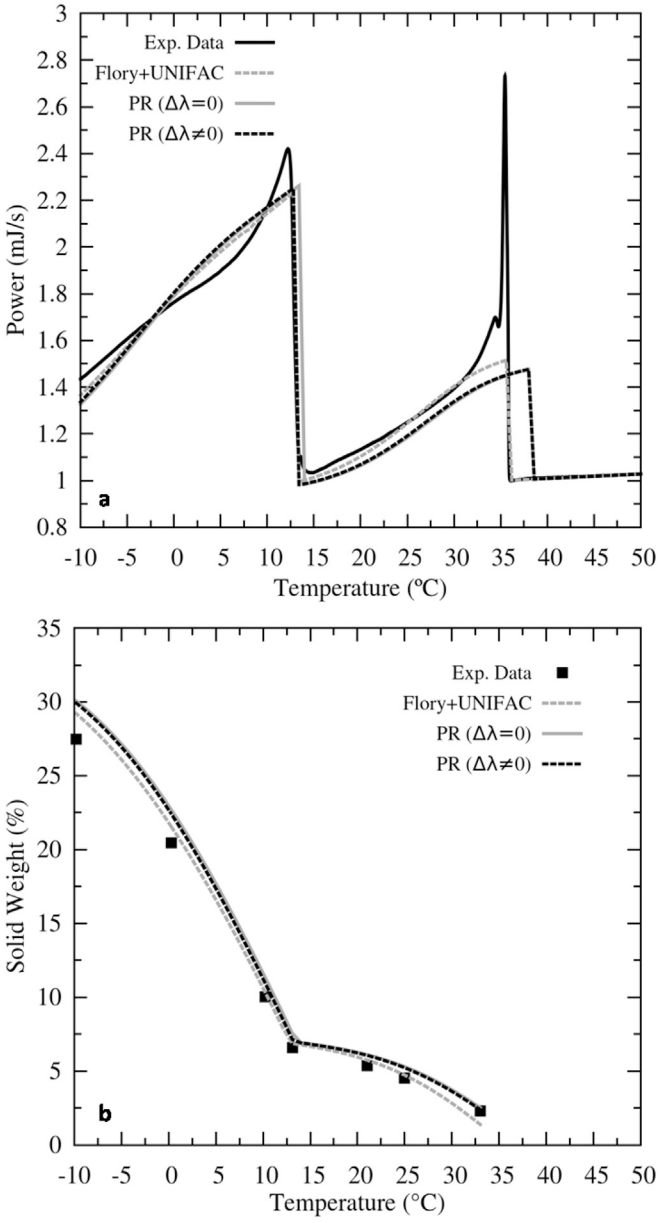


**Fig. 6.** Bim 5 **(a)** DSC and **(b)** Solubility data description using three different approaches: modified UNIQUAC for solid phases and Peng-Robinson EoS for the liquid phase; modified UNIQUAC for solid phases and Flory + UNIFAC for the liquid phase; modified UNIQUAC with estimated $\Delta\lambda$ for solid phases and Peng-Robinson EoS for the liquid phase.

calculated through thermodynamic models is expected to be higher than the measured WAT as these models calculate indeed the WDT, which is always higher than the WAT (Hansen et al., 1991). Therefore, the PR model gives more realistic results.

The solubility curves displayed in Fig. 4 confirm the similar prediction observed in DSC using the Flory + UNIFAC and PR models for *Bim 0*. The average absolute deviations between experimental and calculated solubilities, obtained from Eq. (56), where *Nexp* is the number of experimental data points, are shown in Table 5.

For the bimodal mixtures, the results displayed in Figs. 5–8 also show a good agreement between the experimental and the calculated data. As shown in Table 2, the parameter estimation using the PR model resulted in small negative values of the parameter $\Delta\lambda$, dislocating the calculated DSC curves to the left side. Moreover, the parameters estimated improved the WDT and the solubility predictions for all bimodal mixtures. The parameter estimation also improved the PR model predictions

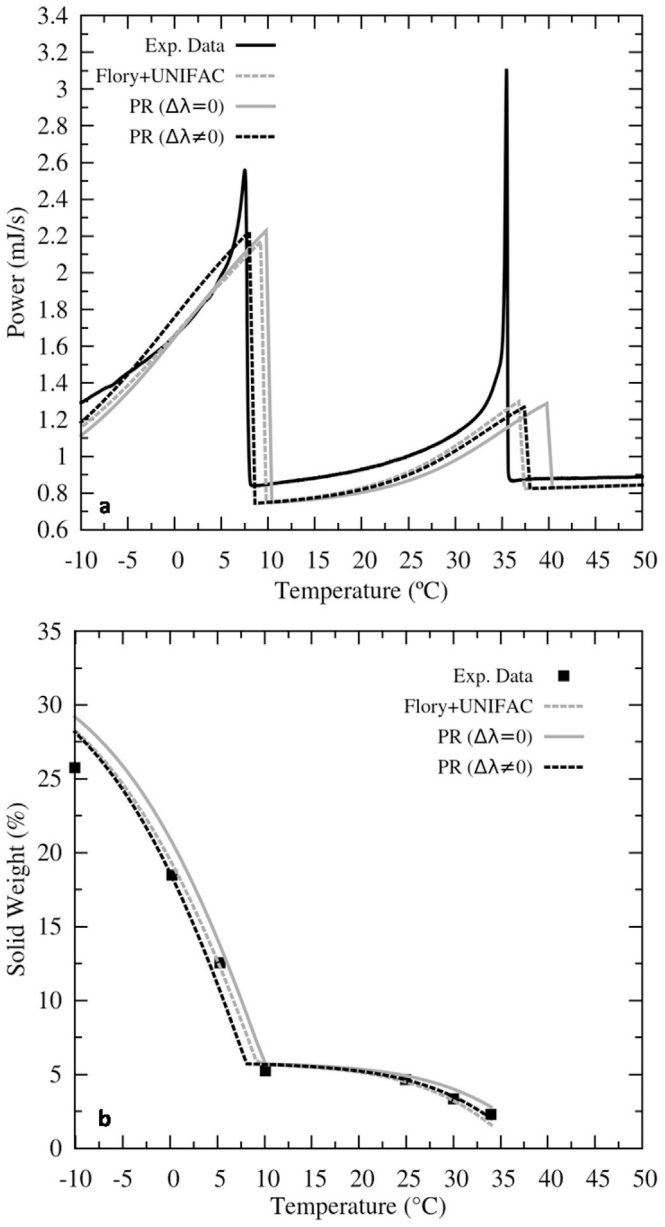


**Fig. 7.** Bim 9 **(a)**DSC and **(b)** Solubility data description using three different approaches: modified UNIQUAC for solid phases and Peng-Robinson EoS for the liquid phase; modified UNIQUAC for solid phases and Flory + UNIFAC for the liquid phase; modified UNIQUAC with estimated $\Delta\lambda$ for solid phases and Peng-Robinson EoS for the liquid phase.

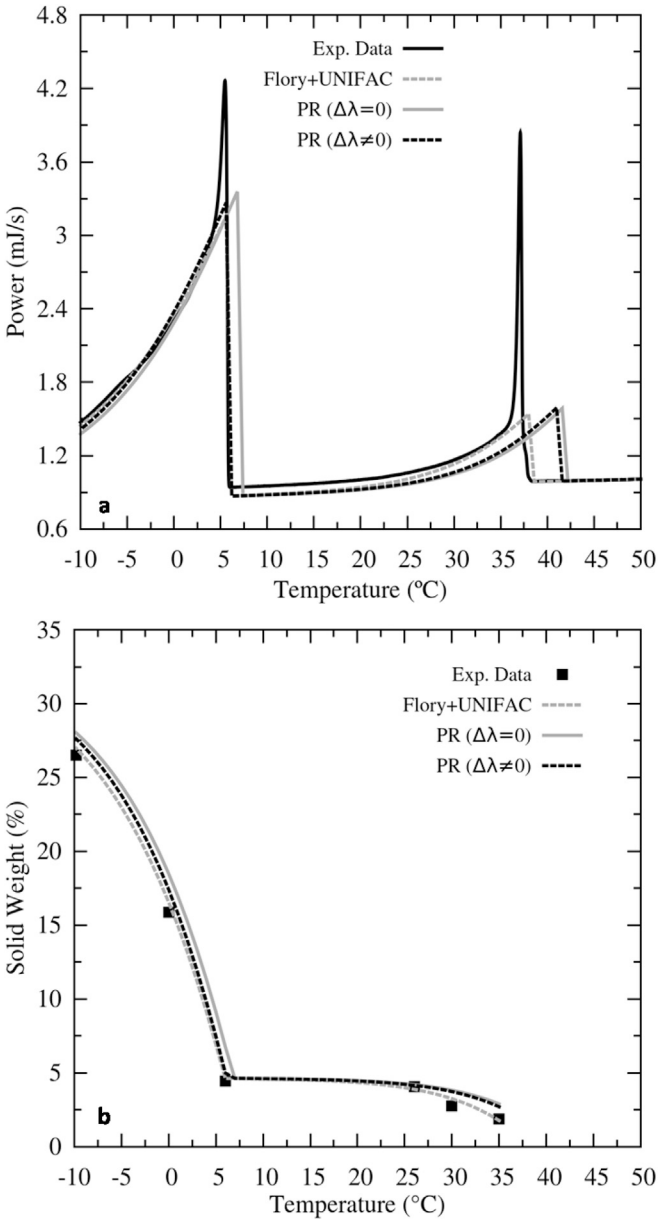


**Fig. 8.** Bim 13 **(a)** DSC and **(b)** Solubility data description using three different approaches: modified UNIQUAC for solid phases and Peng-Robinson EoS for the liquid phase; modified UNIQUAC for solid phases and Flory + UNIFAC for the liquid phase; modified UNIQUAC with estimated $\Delta\lambda$ for solid phases and Peng-Robinson EoS for the liquid phase.

**Table 2**
Parameter estimation results (PR).

| Mixture | *Bim 0* | *Bim 3* | *Bim 5* | *Bim 9* | *Bim 13* |
|---|---|---|---|---|---|
| $\Delta\lambda$ | 0.00014 | −0.00245 | −0.00207 | −0.01294 | −0.00477 |

**Table 3**
Experimental and calculated wax disappearance temperatures (WDT).

| Mixture | *Bim 0* | *Bim 3* | *Bim 5* | *Bim 9* | *Bim 13* |
|---|---|---|---|---|---|
| *Texp* (°C) | 35.60 | 36.50 | 37.22 | 38.18 | 39.66 |
| PR + UNIQUAC ($\Delta\lambda = 0$) | 36.65 | 37.77 | 38.42 | 39.90 | 41.87 |
| PR + UNIQUAC ($\Delta\lambda \neq 0$) | 36.67 | 37.41 | 38.11 | 37.99 | 41.16 |
| PR + IdealSolidSolution | 42.44 | 42.83 | 43.02 | 43.43 | 44.05 |
| PR + Multisolid | 31.94 | 32.90 | 33.53 | 35.14 | 38.00 |
| Flory-UNIFAC + UNIQUAC | 34.08 | 35.08 | 35.65 | 36.91 | 38.51 |

**Table 4**
Deviations between experimental and calculated wax disappearance temperatures (WDT).

| Mixture | *Bim 0* | *Bim 3* | *Bim 5* | *Bim 9* | *Bim 13* |
|---|---|---|---|---|---|
| PR + UNIQUAC ($\Delta\lambda = 0$) | 1.05 | 1.27 | 1.20 | 1.72 | 2.21 |
| PR + UNIQUAC ($\Delta\lambda \neq 0$) | 1.07 | 0.91 | 0.89 | −0.19 | 1.50 |
| PR + IdealSolidSolution | 6.84 | 6.33 | 5.80 | 5.25 | 4.39 |
| PR + Multisolid | −3.66 | −3.60 | −3.69 | −3.04 | −1.66 |
| Flory-UNIFAC + UNIQUAC | −1.52 | −1.42 | −1.57 | −1.27 | −1.15 |

**Table 5**
Average absolute deviations, *Dev*, between experimental and calculated solubilities.

| Mixture | *Bim 0* | *Bim 3* | *Bim 5* | *Bim 9* | *Bim 13* |
|---|---|---|---|---|---|
| PR + UNIQUAC ($\Delta\lambda = 0$) | 0.8445 | 0.9772 | 1.2716 | 1.2464 | 1.4467 |
| PR + UNIQUAC ($\Delta\lambda \neq 0$) | 0.8573 | 0.8475 | 1.0586 | 0.7575 | 0.8495 |
| Flory-UNIFAC + UNIQUAC | 0.4957 | 0.7767 | 0.7093 | 0.7173 | 0.3425 |

for the second peak in the mixtures *Bim 5*, *Bim 9* and *Bim 13*. As observed for *Bim 0*, the PR model results are quite similar to the Flory + UNIFAC results, indicating that the PR model is able to model the thermodynamic effects in the DSC experiments and provide good descriptions of WDT and solubility curves for the SLE involving paraffins.

These results obtained are very important to predict the paraffin precipitation for real oils because with the use of the Peng-Robinson EoS for describing the liquid phase it is possible to improve the thermodynamic model by tuning the EoS parameters, besides taking the pressure effects into consideration. In addition, the EoS is the approach conventionally used by the petroleum industry.

Concerning the methodology proposed for the DSC simulation, the rigorous thermodynamic path for the enthalpy calculation is showed to be accurate for describing the heat flows and phase transitions measured in the DSC experiments for the mixtures studied in this work.

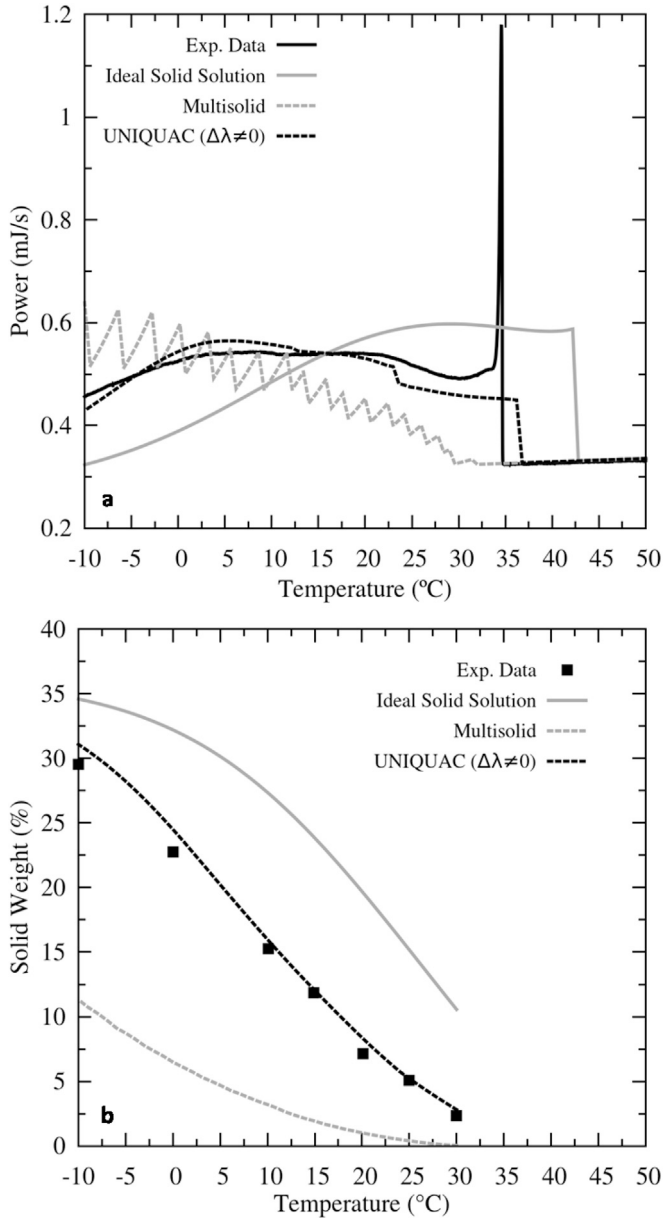


**Fig. 9.** Bim 0 **(a)** DSC and **(b)** Solubility data description using Peng-Robinson EoS for the liquid phase and comparing three different models for solid phases: modified UNIQUAC with estimated $\Delta\lambda$, ideal solid solution and multisolid.

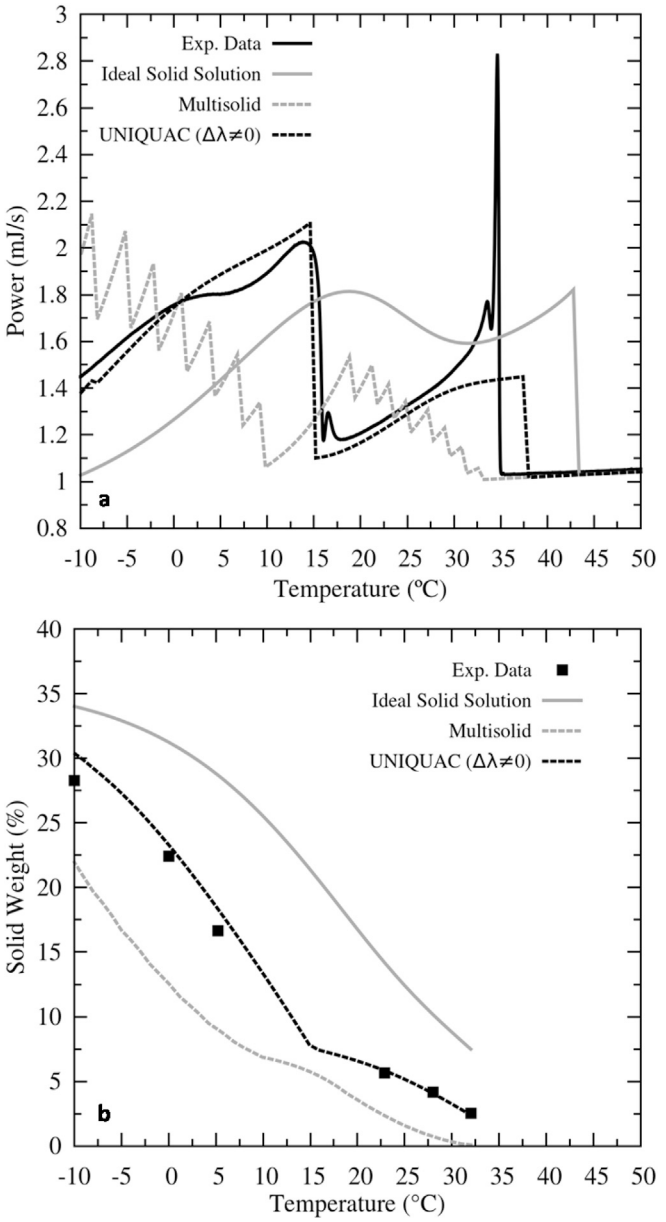


**Fig. 10.** Bim 3 **(a)**DSC and **(b)**solubility data description using Peng-Robinson EoS for the liquid phase and comparing three different models for solid phases: modified UNIQUAC with estimated $\Delta\lambda$, ideal solid solution and multisolid.

$$Dev = \sum_{p=1}^{Nexp} \frac{\left| wt_p^{exp} - wt_p^{calc} \right|}{Nexp} \quad (56)$$

### 4.2. Solid model evaluation

DSC simulations and solubility curves calculated with the solid solution, ideal solid solution and multisolid models are compared with experimental data in Figs. 9–13. No discussion is held about number of solid phases and their compositions because the corresponding experimental data was not assessed. Besides, the main objective here is to show that the DSC curves can be calculated through well-established models for well characterized samples. The Peng-Robinson EoS was used to calculate the fugacities of the components in the liquid phase for the three models. For the solid phase, the multisolid model uses the multi-pure-solid approach, the ideal solid solution uses the supposition of an ideal solid phase, and the solid solution model uses the modified UNIQUAC model with the parameter $\Delta\lambda$ estimated in this work. Because the samples studied here are well characterized, the multisolid model implemented treats each solid phase as a pure paraffin, although Lira-Galeana et al. (1996) and Pan et al. (1997) have suggested the application of the model using pseudo-components. Further work is required to make a complete comparison between the multisolid model (using pseudo-components) and the solid solution model.

Figs. 9–13 show that the DSC results are the same at temperatures above the WAT for the three models, where the system is completely in the liquid phase. The good agreement to experimental results indicates that the correlations used to estimate the ideal gas heat capacities, $Cp^{ig}_{i,pure}$, are accurate.

The differences in the DSC simulations begin when the WDT's are predicted by each model. As shown in Tables 3 and 4, the multisolid model underestimated and the ideal solid solution model overestimated the WDT for the five mixtures studied. These models can be adjusted to

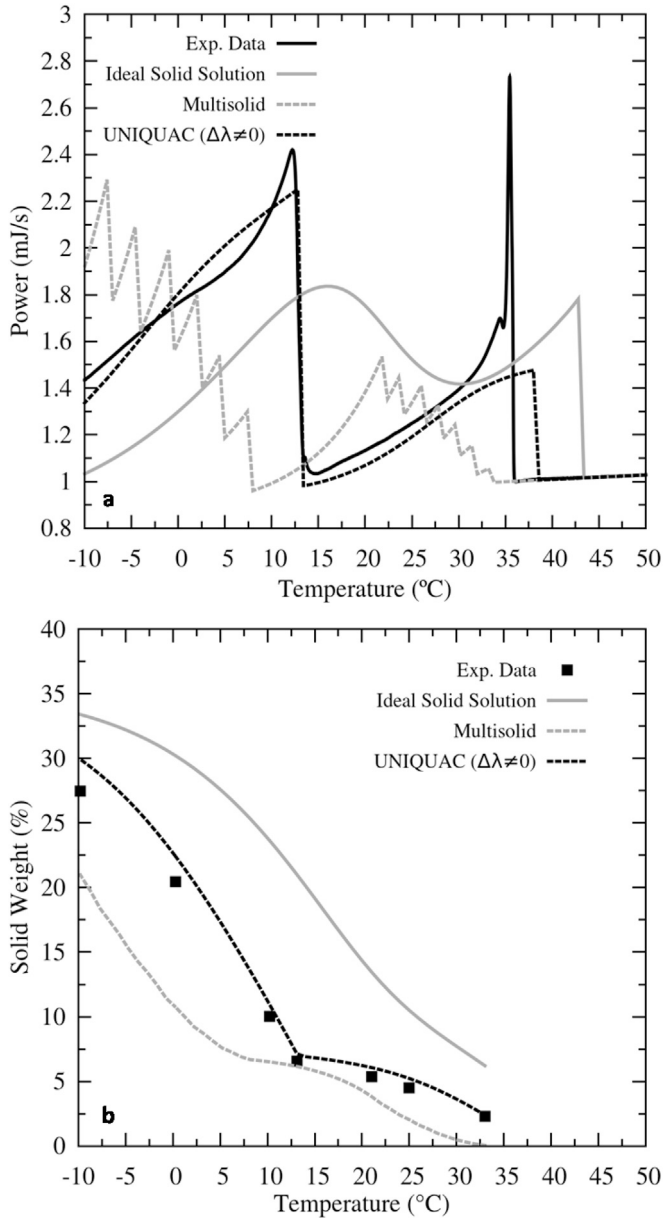


**Fig. 11.** Bim 5 **(a)** DSC and **(b)** Solubility data description using Peng-Robinson EoS for the liquid phase and comparing three different models for solid phases: modified UNIQUAC with estimated $\Delta\lambda$, ideal solid solution and multisolid.

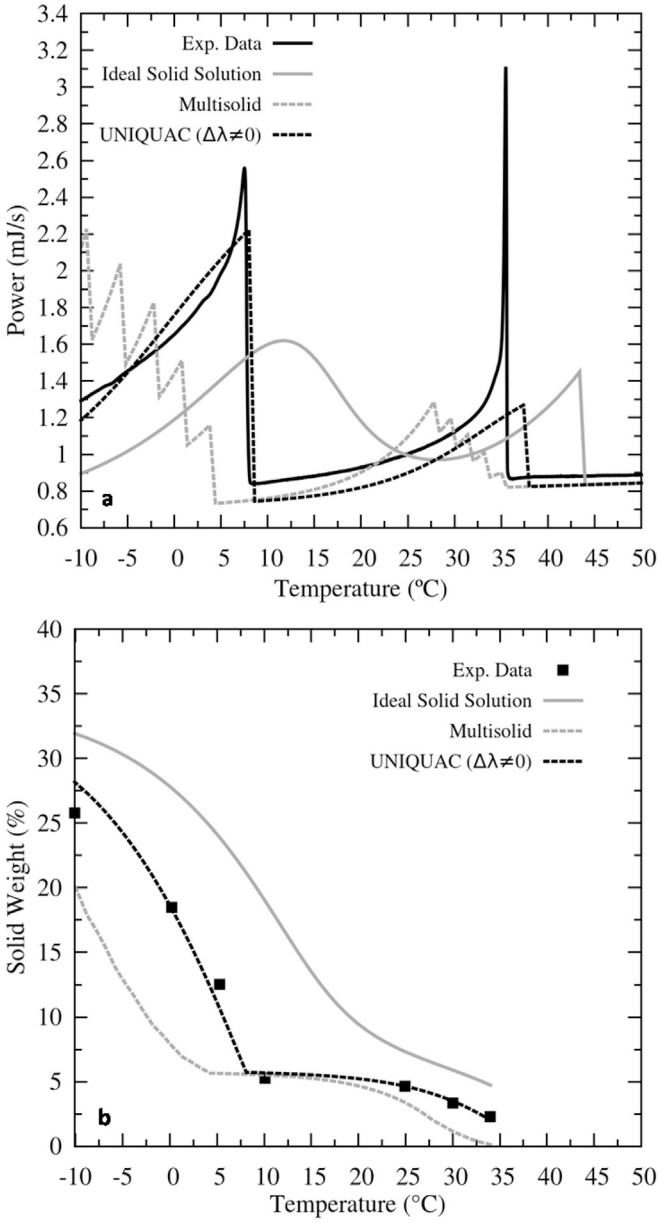


**Fig. 12.** Bim 9 **(a)** DSC and **(b)** Solubility data description using Peng-Robinson EoS for the liquid phase and comparing three different models for solid phases: modified UNIQUAC with estimated $\Delta\lambda$, ideal solid solution and multisolid.

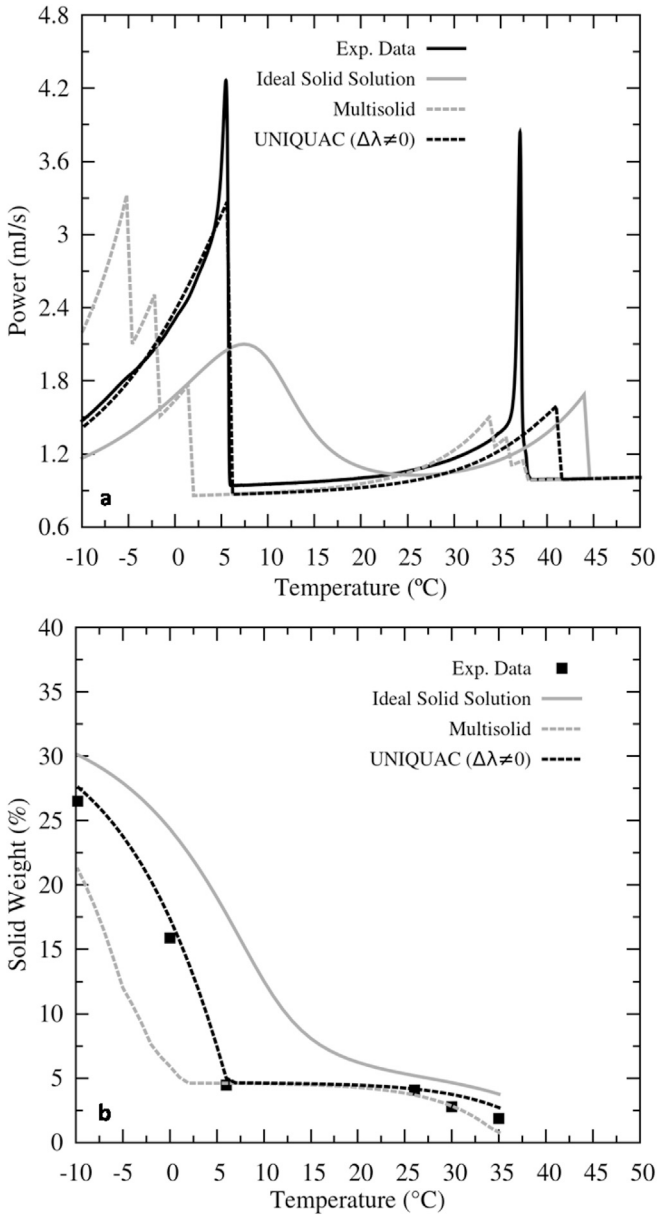


**Fig. 13.** Bim 13 **(a)**DSC and **(b)**Solubility data description using Peng-Robinson EoS for the liquid phase and comparing three different models for solid phases: modified UNIQUAC with estimated $\Delta\lambda$, ideal solid solution and multisolid.

improve the WDT prediction, however, either the physical properties of the pure paraffins or the composition itself are used to tune the models, which is not physically justifiable. Furthermore, in this case only the WDT will be adjusted, what doesn't ensure good predictions for the entire solubility curve.

Contrary to the solid solution model, the simulated DSC using the multisolid and ideal solid solution models are not in agreement with the trends presented in the experimental data. Moreover, the multisolid model underestimated and the ideal solid solution model overestimated the amount of paraffin precipitated.

Then, taking into consideration the conditions under evaluation, all the results indicate that the assumption of a solid solution is more adequate to model the SLE than the assumptions of neither a multi-pure-solid phase, the way it was implemented here, nor an ideal solid solution. It also becomes evident that the solubility curves alone are not a good comparison to differentiate the solid models.

## 5. Conclusion

As oil production pushes the boundaries of hostile environments, wax deposition simulation assumes a major role in production system design. These simulations are dependent on an accurate thermodynamic SLE model, which renders the solubility curve. To improve model tuning, a strategy is developed through the evaluation of different models both for liquid and solid phases.

To allow a wide application of this strategy, a new DSC thermogram calculation scheme is proposed, where all of the non-idealities of the different phases are used in the heat flux calculation, as well as an ideal gas reference state was set for all components in all phases. As expected, this result indicates that the non-idealities involved in pure paraffinic systems are small when compared to the heats of phase change. It also points out that DSC experiments at slow enough rates are completely dominated by thermodynamic phenomena, indicating that the proposed strategy represents a significant improvement on relating information from DSC curves to solubility ones. The extrapolation of this new scheme to a multiphase condition is then straightforward.

In order to make the proposed strategy readily applicable to the oil industry, a liquid model based on EoS was evaluated, since this approach is already widely used. The simulation of DSC thermograms was used to compare the performance of the Peng-Robinson EoS in wax precipitation calculations to the Flory and modified UNIFAC models. Results show that the EoS model can be used with little or no losses when compared to the Flory and UNIFAC model. The model tuned to the experimental DSC thermogram renders a solubility curve in agreement with the experimental results within experimental errors.

The proposed strategy also allowed one to compare different solid models. A suitable SLE model should be able to correctly predict the experimental solubility curve as well as the DSC thermogram. The presented results showed that, although the different models evaluated render solubility curves that seem to differ only in values and that might be adjustable, the differences observed in the thermograms allows one to separate these models further. The DSC thermogram is an experimental result directly related to the solubility curve. In this sense, the differences pointed out among the solid models evaluated affect directly their ability to be used in the current wax deposition model. It is an immediate conclusion that the solid solution model renders more accurate solubility curves, which cannot be tuned in the other models evaluated.

## Acknowledgement

The authors acknowledge ANP-PETROBRAS program for the financial support.

## List of symbols

| | |
|---|---|
| $Q$ | heat |
| $H$ | enthalpy |
| $t$ | time |
| $Nmol$ | number of moles of the mixture |
| $T$ | temperature |

| | |
|---|---|
| $P$ | pressure |
| $Np$ | number of phases |
| $Nc$ | number of components |
| $V$ | volume |
| $Cp$ | heat capacity |
| $x$ | molar fraction |
| $f$ | fugacity |
| $K$ | equilibrium ratio |
| $r$, $q$ | structural parameters |
| $G$ | Gibbs free energy |
| $Z$ | coordination number |
| $CN$ | number of carbon atoms |
| $MW$ | molecular weight |
| $wt$ | weight fraction of solid |
| $F$ | residuals of the Newton method |
| $tm$ | modified tangent plane distance |
| $W$ | stability variable |
| $Nexp$ | number of experimental data points |

*Superscripts*

| | |
|---|---|
| $n$, $m$ | phase index |
| $f$ | fusion |
| $tr$ | transition |
| $ig$ | ideal gas |
| $R$ | residual property |
| $S$ | solid phase |
| $L$ | liquid phase |
| E | excess property |
| $res$ | residual |
| $comb\text{-}fv$ | combinatorial-free volume |
| $sub$ | sublimation |
| $vap$ | vaporization |

*Subscripts*

| | |
|---|---|
| $i$, $j$, $w$ | component index |
| $p$ | experimental data points index |
| $0$ | ideal gas reference state |

*Greek letters*

| | |
|---|---|
| $\Delta$ | variation |
| $\beta$ | phase fraction |
| $\gamma$ | activity coefficient |
| $\tau$, $\theta$, $\Phi$ | modified UNIQUAC parameters |
| $\lambda$ | interaction energy |
| $\varphi$ | fugacity coefficient |
| $\delta$ | kronecker delta |

*Accent*

| | |
|---|---|
| $\bar{}$ | molar property |
| $\underline{}$ | vector |
| $\hat{}$ | property in the mixture |
| $\underline{\underline{}}$ | matrix |

*Abbreviations*

| | |
|---|---|
| DSC | differential scanning calorimetry |
| EGE | excess Gibbs energy |
| EoS | equation of state |
| PVT | pressure, volume, temperature |
| SLE | solid-liquid equilibria |
| WAT | wax appearance temperature |
| WDT | wax disappearance temperature |
| TPD | tangent plane distance |

## References


Abrams, D.S., Prausnitz, J.M., 1975. Statistical thermodynamics of liquid mixtures: a new expression for the excess Gibbs energy of partly or completely miscible systems. AIChE J. 21, 116–128.

Azevedo, L.F.A., Teixeira, A.M., 2003. A critical review of the modeling of wax deposition mechanisms. Petroleum Sci. Technol. 21, 393–408.

Banki, R., Hoteit, H., Firoozabadi, A., 2008. Mathematical formulation and numerical modeling of wax deposition in pipelines from enthalpy–porosity approach and irreversible thermodynamics. Int. J. Heat Mass Transf. 51, 3387–3398.

Chiavaro, E., 2015. Differential Scanning Calorimetry - Application in Fat and Oil Technology. CRC Press, Florida.

Coutinho, J.A.P., Andersen, S.I., Stenby, E.H., 1995. Evaluation of activity coefficient models in prediction of alkane solid-liquid equilibria. Fluid Phase Equilib. 103, 23–39.

Coutinho, J.A.P., Knudsen, K., Andersen, S.I., Stenby, E.H., 1996. A local composition model for paraffinic solid solutions. Chem. Eng. Sci. 51, 3273–3282.

Coutinho, J.A.P., Daridon, J.L., 2005. The limitations of the cloud point measurement techniques and the influence of the oil composition on its detection. Petroleum Sci. Technol. 23, 1113–1128.

Coutinho, J.A.P., Mirante, F., Pauly, J., 2006. A new predictive UNIQUAC for modeling of wax formation in hydrocarbon fluids. Fluid Phase Equilib. 247, 8–17.

Dauphin, C., Daridon, J.L., Coutinho, J.A.P., Baylere, P., Potin-Gautier, M., 1999. Wax content measurements in partially frozen paraffinic systems. Fluid Phase Equilib. 161, 135–151.

Fleming, F.P., Daridon, J.L., Azevedo, L.F.A., Pauly, J., 2017. Direct adjustment of wax thermodynamic model parameter to Micro Differential Scanning Calorimetry thermograms. Fluid Phase Equilib. 436, 20–29.

Hansen, A.B., Larsen, E., Pedersen, W.B., Nielsen, A.B., 1991. Wax precipitation from North Sea crude oils. 3. Precipitation and dissolution of wax studied by differential scanning calorimetry. Energy & Fuels 5, 914–923.

Hansen, J.H., Fredenslund, A., Pedersen, K.S., Ronningsen, H.P., 1988. A thermodynamic model for predicting wax formation in crude oils. AIChE J. 34, 1937–1942.

Hooke, R., Jeeves, T.A., 1961. "Direct search" solution of numerical and statistical problems. J. Assoc. Comp. Mach. 8, 212–229.

Huang, Z., Zheng, S., Fogler, H.S., 2015. Wax Deposition: Experimental Characterizations, Theoretical Modeling, and Field Practices. CRC Press, Florida.

Ji, H.-Y., Tohidi, B., Danesh, A., Todd, A.C., 2004. Wax phase equilibria: developing a thermodynamic model using a systematic approach. Fluid Phase Equilib. 216, 201–217.

Larsen, B.L., Fredenslund, A., Rasmussen, P., 1987. A modified UNIFAC group-contribution model for prediction of phase equilibria and heats of mixing. Ind. Eng. Chem. Res. 26, 2274–2286.

Lira-Galeana, C., Firoozabadi, A., Prausnitz, J.M., 1996. Thermodynamics of wax precipitation in petroleum mixtures. AIChE J. 42, 239–248.

Marano, J.J., Holder, G.D., 1997. General equation for correlating the thermophysical properties of n-paraffins. n-Olefins. And other homologous series. 2. Asymptotic behavior correlations for PVT properties. Ind. Eng. Chem. Res. 36, 1895–1907.

Michelsen, M.L., 1982. The isothermal flash problem. part I. stability. Fluid Phase Equilib. 9, 1–19.

Morgan, D.L., Kobayashi, R., 1994. Extension of Pitzer CSP models for vapor pressures and heats of vaporization to long-chain hydrocarbons. Fluid Phase Equilib. 94, 51–87.

Pan, H., Firoozabadi, A., Fotland, P., 1997. Pressure and composition effect on wax precipitation: experimental data and model results. SPE Prod. Facil. 11, 250–259.

Passut, C.A., Danner, R.P., 1972. Correlation of ideal gas enthalpy, heat capacity, and entropy. Ind. Eng. Chem. Process Des. Dev. 11, 543–546.

Peng, D.-Y., Robinson, D.B., 1976. A new two-constant equation of state. Ind. Eng. Chem. Fundam. 15, 59–64.

Won, K.W., 1986. Thermodynamics for solid-liquid-vapor equilibria: wax phase formation from heavy hydrocarbon mixtures. Fluid Phase Equilib. 30, 265–279.

Ziervogel, R.G., Poling, B.E., 1983. A simple method for constructing phase envelopes for multicomponent mixtures. Fluid Phase Equilib. 11, 127–135.